ASIAN J NAT PROD BIOCHEM
Volume 24, Number 1, June 2026
Pages: 13

P-ISSN: 2775-4189
E-ISSN: 2775-4197
https://doi.org/10.13057/biofar/f240104

Hepatoprotective activity, phytochemical profile and molecular docking of flavonoids of *Thesium viride*

SANI SHEHU[1], MUSTAPHA ABDULLAHI[2], UWAISU ILIYASU[1], ALAA AHMAD HAMDY[3], YUSHAU MUSA HADI[1], UMAR HABIB DANMALAM[4], HEMN STAR[5], KHALIS MOHAMMED SHAHADHA[6], ABDULLAHI ALIYU[7,♥], ABDULRAHMAN MAHMOUD DOGARA[8,♥♥], ATEEQ AHMED AL-ZAHRANI[9], MARIAM SALEH ALGHAMDI[10]

[1]Department of Pharmacognosy and Drug Development, Faculty of Pharmaceutical Sciences, Kaduna State University. P.M.B. 2339, Tafawa Balewa Way, Kabala Coastain, Kaduna 800283, Kaduna State, Nigeria
[2]Department of Pure and Applied Chemistry, Faculty of Physical Sciences, Kaduna State University. P.M.B. 2339, Tafawa Balewa Way, Kabala Coastain, Kaduna 800283, Kaduna State, Nigeria
[3]Derabon Primary Health Center, Duhok Directorate of Health. MOH KRG, Iraq
[4]Department of Pharmacognosy and Drug Development, Faculty of Pharmaceutical Sciences, Ahmadu Bello University. Zaria 810211, Kaduna, Nigeria
[5]Nursing Department, Tishk International University. Sulaimanyah, Kurdistan Region, Iraq
[6]Department of Chemistry and Biochemistry, College of Medicine, Ninevah University. Mosul, Iraq
[7]Department of Veterinary Medicine, College of Applied and Health Sciences, A'Sharqiyah University. PO Box 42, Postal code 400, Ibra, Sultanate of Oman. Tel.: +968-9772-9166, ♥email: abdullahi.aliyu@asu.edu.om
[8]Department of Biology Education, Tishk International University. Erbil, Iraq. Tel.: +964-751-159-9240, ♥♥email: abdulrahman.mahmud@tiu.edu.iq
[9]Department of Chemistry, University College at Al-Qunfudhah, Umm Al-Qura University. Alkhaldiyah, Al Qunfudhah 28821, Saudi Arabia
[10]Department of Environmental Sciences, College of Science, University of Jeddah. P.O. Box 80237, Jeddah 21589, Saudi Arabia

Manuscript received: 7 December 2025. Revision accepted: 16 May 2026.

Abstract. *Shehu S, Abdullahi M, Iliyasu U, Hamdy AA, Hadi YM, Danmalam UH, Star H, Shahadha KM, Aliyu A, Dogara AM, Al-Zahrani AA, Alghamdi MS. 2026. Hepatoprotective activity, phytochemical profile and molecular docking of flavonoids of* Thesium viride*. Asian J Nat Prod Biochem 24 (1): f240104. https://doi.org/10.13057/biofar/f240104.* Liver disease is a major global health challenge. Medicinal plants such as *Thesium viride* can be used as alternatives, considering the traditional use of *T. viride* in liver management and the considerable drawbacks of current conventional therapy. This study aimed to evaluate the hepatoprotective effects of the *T. viride* fraction in vivo and in silico to confirm its traditional usage. Wistar rats (140-180 g) were pretreated with a flavonoid-rich fraction (200 or 400 mg/kg) seven days before carbon tetrachloride (CCl_4)-induced hepatotoxicity, and liver function (ALT, AST, and ALP), oxidative stress biomarkers (MDA, CAT, and SOD), and histopathology (using a semi-quantitative scoring technique) were then evaluated to determine hepatoprotective efficacy. High-Performance Liquid Chromatography/Mass Spectrometry (HPLC/MS) analysis of the fraction was performed, and molecular docking was performed on the fraction. Pretreatment increased liver indices in a dose-dependent manner, decreased liver enzymes and lipid peroxidation (MDA), and promoted the recovery of antioxidant defenses (CAT and SOD). There was a significant reduction in necrosis, ballooning, and congestion, as observed via histology. Molecular docking against the Keap1 protein (PDB: 4L7B) revealed that all 11 identified compounds formed highly stable ligand–protein complexes; in particular, isorhamnetin-3-galactoside-7-rhamnoside had higher binding affinities than the reference ligand did, suggesting its predicted hepatoprotective activity. The flavonoid-rich fraction of *T. viride* has significant hepatoprotective potential, making it an attractive candidate for future biological validation. Further investigations are warranted to evaluate the long-term safety and efficacy of the fraction in chronic liver disease models.

Keywords: Antioxidant, carbon tetrachloride, flavonoids, liver, *Thesium viride*

Abbreviations: ALT: Alanine Aminotransferase, ALP: Alkaline Phosphatase, AST: Aspartate Aminotransferase, CADD: Computer-Aided Drug Design, CAT: Catalase, ESI: Electrospray Ionization, H_2O_2: Hydrogen peroxide, HPLC/MS: High-Performance Liquid Chromatography/Mass Spectrometry, LD_{50}: Lethal Dose, 50%, MASLD: Metabolic Dysfunction-Associated Steatotic Liver Disease, MDA: Malondialdehyde, mg/kg: Milligram per Kilogram, SAS: Statistical Analysis System, SOD: Superoxide Dismutase, *T. viride: Thesium viride,* TLC: Thin-Layer Chromatography

INTRODUCTION

Acute liver injury, which is commonly caused by toxic, viral, or ischemic agents, is a serious clinical and public health issue because of its rapid progression and may lead to severe outcomes (Yang 2020). The liver, the largest internal organ, is involved in critical metabolic, detoxification, and synthetic processes essential for physiological homeostasis. The mortality rates caused by liver disease are high worldwide, with approximately 2 million deaths occurring every year (Paik et al. 2020). This total covers 1 million deaths due to the complications of cirrhosis and another 1 million deaths due to viral hepatitis and hepatocellular carcinoma (Liu and Chen 2022). This tremendous burden is further complicated by the fact that the etiology of hepatic pathologies is diverse and complex

and includes chronic viral infections (hepatitis B and C), steatotic liver disease (MASLD) related to metabolic dysfunction, autoimmune diseases, exposure to environmental toxins, excessive alcohol intake, and drug reactions (Prata et al. 2020; Huang et al. 2025). The pathogenesis of liver disease is often characterized by an insidious progression of the first injury and steatosis into inflammation (steatohepatitis), fibrosis, cirrhosis, and, finally, failure of the organ or the development of cancer. The main clinical issue is the extraordinary functional reserve and regenerative capacity of the organ, which, in many cases, allows substantial damage to go unnoticed until it progresses to full-scale, and frequently beyond repair, decompensated cirrhosis or malignancy (Tapper and Parikh 2023). It can be very insidious in its progression and may cause significant harm even before symptoms manifest. The liver is central to metabolism and detoxification; therefore, it is an organ particularly susceptible to damage. In addition to modern medicine, no treatments are fully effective, and they cannot be sure to restore hepatic function, protect organs holistically, or aid in the regeneration of hepatocytes (Chattopadhyay 2003; Venmathi et al. 2022).

The commonly used treatment options, which include steroids, antiviral drugs, and vaccines, are usually expensive and carry the risk of side effects (Venmathi et al. 2022). It has led to increasing interest in herbal medicine as an alternative approach, an ancient practice founded on the empirical experience of many cultures that have used the therapeutic effects of many plants to maintain liver health and treat liver-related diseases (Negi et al. 2008). Thus, scientific research is increasingly looking beyond traditional avenues to develop safer and more convenient forms of therapy. Plants that have a long history of traditional use for liver ailments with anecdotal support. The historical uses of these products are based on observations of their hepatoprotective properties, providing a theoretical basis for modern phytochemical study of plant-derived products for liver therapeutics. In turn, rational confirmation of these classical assertions through up-to-date pharmacological and clinical research is crucial for distinguishing ethnomedicine from evidence-based drug discovery for hepatic diseases.

Computer-Aided Drug Design (CADD) has become an indispensable tool in the quest to make the drug discovery process faster yet more economical (Kaur et al. 2025). Molecular docking virtual screening is one of its many methods. It is central to structure-based drug design (SBDD), in which small molecules are predicted to bind to a target protein despite their size, optimal orientation, and binding affinity, using computational methods (Kaur et al. 2025).

Thesium viride A.W. Hill is a hemiparasite subshrub belonging to the family Santalaceae and is widely distributed in Africa, Madagascar, and South America (Zhigila et al. 2020). The plant is used to treat jaundice, liver enlargement, and splenomegaly (Shehu et al. 2017; Abdulrahman et al. 2022). Nevertheless, preliminary investigations have identified bioactive compounds in crude extracts (Lombard et al. 2020; Dogara et al. 2024). The hepatoprotective effect of its flavonoid-enriched fraction has not been investigated. These compounds are widely known for their powerful antioxidant, anti-inflammatory, antifibrotic, and antiapoptotic effects (Agati et al. 2020). Therefore, the present study aimed to profile flavonoid-rich extracts of *T. viride* using LC-MS/MS to identify the bioactive constituents responsible for hepatoprotection and to determine the binding potential of *T. viride* to individual proteins involved in liver pathogenesis.

MATERIALS AND METHODS

Plant collection and extraction

The aerial part of the plant was collected from the wild in Kaduna State, Nigeria. It was identified and authenticated with voucher number KASU/PCG/HERB/300 at the Herbarium Unit of the Department of Pharmacognosy and Drug Development, Kaduna State University, Kaduna. This powdered plant material (1 kg) was mixed with 70% (v/v) aqueous ethanol in a glass jar and shaken intermittently for 72 hours. The extract was filtered through muslin cloth, then through Whatman No. 1 filter paper. This pooled filtrate was concentrated at reduced pressure at 30°C in a rotary evaporator (Buchi, Switzerland), and the remaining solvent was dried thoroughly in a water bath at 60°C to obtain a greenish-brown crude extract (Shehu et al. 2025).

Fractionation of the crude extract

The aqueous ethanol extract (130 g) was suspended in distilled water (300 mL) and subjected to sequential liquid-liquid partitioning to separate the constituents depending on the polarity (Shehu et al. 2025). A separating funnel was used to exhaustively and successively separate the suspension with n-hexane, ethyl acetate, and n-butanol. The fractions were obtained individually. The ethyl acetate fraction had the highest flavonoid content and was chosen for further study. The ethyl acetate fraction was concentrated under reduced pressure at 30°C to yield a dry, solid residue, which was further purified (Etame et al. 2019).

Column chromatography of the flavonoid-rich fraction of *T. viride*

Approximately 2 g of silica gel was dried and preadsorbed to the fraction (1 g). The mixture was then placed on the column and eluted first with 200 mL of n-hexane (100%) at 2 mL/min to remove nonpolar impurities (Shehu et al. 2025). Twenty-milliliter aliquots were taken. The polarity then gradually increased to 90:10, 80:20, 70:30, 60:40, and 50:50 (hexane/ethyl acetate, v/v). Further polar additions of ethyl acetate, individually and finally ethyl acetate/methanol mixtures (up to 10% methanol), were made as necessary, as directed by TLC monitoring [silica gel, UV 254/366 nm, detection using Natural Product/PEG reagent]. Fractions with similar R_f values and spotting patterns resulted in bulky fractions F, G, and H

(equivalent to flavonoid-rich zones). Preparative TLC was also used to purify further the bulk fractions F, G, and H.

Animals and housing

Healthy adult female Wistar rats (weight: 140-180 g) were obtained from the Department of Pharmacology and Therapeutics. The animals were housed in standard polypropylene cages under controlled environmental conditions (temperature: 22±3°C; relative humidity: 50-60%; 12-hour light/dark cycle). They were provided with a standard pellet diet and water ad libitum.

Acute toxicity (LD_{50}) determination

Acute toxicity experiments were conducted to determine the LD_{50} of the flavonoid-rich fraction using a standardized protocol, i.e., the Organization for Economic Cooperation and Development (OECD) (Morris-Schaffer and McCoy 2020). Before the experiment, the rats were randomly assigned to three groups, each with six animals (n=6), and acclimatized to laboratory conditions for two weeks. All groups were fasted overnight before receiving the extract. The extract was formulated in distilled water and administered orally.

Group one: Control (only water).

Group 2: Received 2000 mg of extract/kg body weight (BW).

Group 3: Received 5000 mg of extract per kg body weight (BW).

Post-treatment observation period

After administration of the extracts, animals were monitored for 4 hours to assess immediate evidence of toxicity, such as behavioral changes and mortality. After that, daily observations of all animals were conducted over 14 days to record delayed toxicity, body weight, feeding habits, and any clinical signs. Mortality and the number of deaths were recorded on days 0, 7, and 14.

Experimental design

Healthy male Wistar rats weighing 140-180 g, obtained from the Department of Pharmacology and Therapeutics with ethical clearance ABUCAUC/2021/065, were grouped into four groups of six animals each (4 groups, n=6) (Nagalekshmi et al. 2011). The Wistar rats were randomly divided into four groups (n=6):

In Group I **(**normal control), only vehicle (olive oil, p.o.) was given daily for 7 days, and a single vehicle injection (i.p.) was given on day 8 (Nagalekshmi et al. 2011).

In Group II (Disease Control), the vehicle (p.o.) was administered daily for 7 days, and a single i.p. injection was administered. CCl_4 (1.2 mL/kg of a 40% v/v solution in olive oil, i.p.) was administered on day 8 to induce hepatotoxicity (Nagalekshmi et al. 2011).

Group III (low-dose treatment): The samples were pretreated with the flavonoid-rich fractions at 200 mg/kg (p.o.) daily for 7 days, followed by CCl_4 injection on day 8 (Nagalekshmi et al. 2011).

Group IV (high-dose treatment): The samples were pretreated with the flavonoid-rich fractions at 400 mg/kg (p.o.) daily for 7 days, followed by CCl_4 injection on day 8 (Nagalekshmi et al. 2011).

Histopathological examination

A portion of the liver lobe was preserved in 10% neutral formalin solution for at least 24 h, processed, and paraffin-embedded as per the standard protocol. The liver tissue was fixed in 10% buffered formalin. The tissues were cut into small pieces approximately 1 cm in size and then placed in cassettes containing fresh formalin at a 10:1 fixative-to-tissue ratio for 48 hr. The tissue was processed via dehydration in a series of alcohols. The dehydrant was removed with toluene, which is miscible with the embedding medium paraffin. Finally, the tissues were infiltrated with paraffin in an oven at less than 60°C. The tissues were transferred into molten paraffin blocks. Sections 5 μm in thickness were cut, deparaffinized, dehydrated, and stained with hematoxylin and eosin (H&E). Histopathological examination of the liver was performed by light microscopy at a magnification of ×400 (Abdou et al. 2019; Chowdhury and Mehta 2023). Liver scoring: Histopathological alterations, tissue necrosis, ballooned cells, vacuolation, the presence of a congested central vein, and the infiltration of inflammatory cells were scored as follows: (0) indicates no changes, and (1), (2), and (3) indicate mild, moderate, and severe changes, respectively. The average number of lesions per 10 high-power fields (HPFs) with the X10 objective was counted for each case and recorded (Abdou et al. 2019; Chowdhury and Mehta 2023).

Estimation of biochemical parameters

Alanine aminotransferase (ALT) and aspartate aminotransferase (AST) were measured using the standardized International Federation of Clinical Chemistry (IFCC) kinetic technique, by monitoring the rate of reduction at 340 nm. Alkaline phosphatase (ALP) activity was determined using the p-nitrophenyl phosphate (pNPP) system, in which pNPP is hydrolyzed by ALP, producing a yellow product, which can be measured at 405 nm (Talli et al. 2025). Malondialdehyde (MDA): The degree of lipid peroxidation in the serum was measured via the thiobarbituric acid reactive substances (TBARS) assay. In this technique, MDA reacts with thiobarbituric acid under acidic conditions to form a pink chromogen, which is quantified at 532-535 nm. Catalase (CAT): This activity was measured by observing the breakdown of hydrogen peroxide (H_2O_2). The change in absorbance of H_2O_2 at 240 nm over time was recorded, and the rate of change was proportional to catalase activity.

High-performance liquid chromatography/mass spectrometry (HPLC/MS) analysis

The flavonoid-rich fraction was dissolved in methanol, and separation of the compounds was conducted on an Agilent 6460 Triple Quad LC/MS/HPLC-1290 infinity instrument equipped with an Agilent SB-C18 column (2.1 × 50 mm, 1.8 μm). Acidified water (0.1% formic acid, v/v) and methanol were used as mobile phases A and B, respectively. The gradient elution program was as follows:

0 min, 70% A and 30% B; 30 min, 100% B; 33 min, 100% B; 35 min, 70% A and 30% B; 40 min, 70% A and 30% B. The flow rate was set at 1 ml/min throughout the elution. The flow rate from the HPLC system into the ESI-MS detector was 0.2 mL/min. The injection volume was 10 µL, and the column temperature was maintained at 25°C (Shi et al. 2023).

The HPLC system was coupled to 2 mass spectrometers and operated with electrospray ionization (ESI) in positive mode at a mass resolution of 100-1000, a gas temperature of 250°C, and a gas flow of 16 L/min. The nebulizer pressure was set at 40 psi, a capillary voltage of 3000 V was used, the sheath gas temperature was 4000°C with a sheath gas flow of 12 L/min, and the fragmentor voltage was set at 30-150 V. The spectra of the compounds separated at the end of the elution were searched in the RIKEN MSn spectral database for phytochemicals (ReSpect) and compared with literature data.

In silico hepatoprotective prediction study

The cheminformatics prediction of the identified compounds as hepatoprotectants was performed using the Prediction of Activity Spectra for Substances online tool (PASS Online) at https://way2drug.com/PassOnline/predict.php. The chemical structures of the identified compounds were drawn and uploaded into the online software. The PASS online tool relies on large Machine Learning (ML)-based Quantitative Structure-Activity Relationship (QSAR) models to predict the probability "to be active" (Pa) and probability "to be inactive" (Pi) of organic molecules for several pharmacological properties, including hepatoprotective potential (Mathes et al. 2025).

Molecular docking study

Molegro Virtual Docker (MVD) was used to evaluate the residual interaction between the discovered chemicals and the crystal structure of the K (Abdullahi et al. 2025) elch-like ECH-associated protein (Keap1) domain, which was cocrystallized using (1S,2R)-2-{[(1S)-1-[(1,3-dioxo-1,3-dihydro-2H-isoindol-2-yl)methyl]-3,4-dihydroisoquinolin-2(1H)-yl]carbonyl-cyclohexane carboxylic acid retrieved from the Protein Data Bank (PDB code: 4L7B) at https://www.rcsb.org/structure/4L7B. To assign bonds, bond orders, hybridization, charges, and missing explicit hydrogen atoms in the protein structure, MVD was initially used to create the recovered protein. With a center axis of X: -3.79, Y: 6.71, and Z: -33.07, the best detected active cavity was positioned inside a 15Å radius constraint sphere (Figure 1). The 3D structures of the identified compounds were generated from their 2D structure and energy-minimized. Each compound was assigned a protonation state at physiological pH, and partial atomic charges were calculated using the default MolPro Virtual Docker. The top protein-ligand complexes were visualized via Discovery Studio after the binding affinity scores (MolDock scores) from the docking simulations were obtained (Abdullahi et al. 2024).

Statistical analysis

All experiments were performed in triplicate, and the findings are expressed as the mean ± Standard Deviation (SD) and were analyzed using Statistical Analysis System (SAS) software (University version 9.4). Statistical significance was evaluated by one-way Analysis of Variance (ANOVA), followed by Dunnett's multiple comparison test, and the results were compared between the positive (*) and negative (#) groups at the $p<0.001$ level.

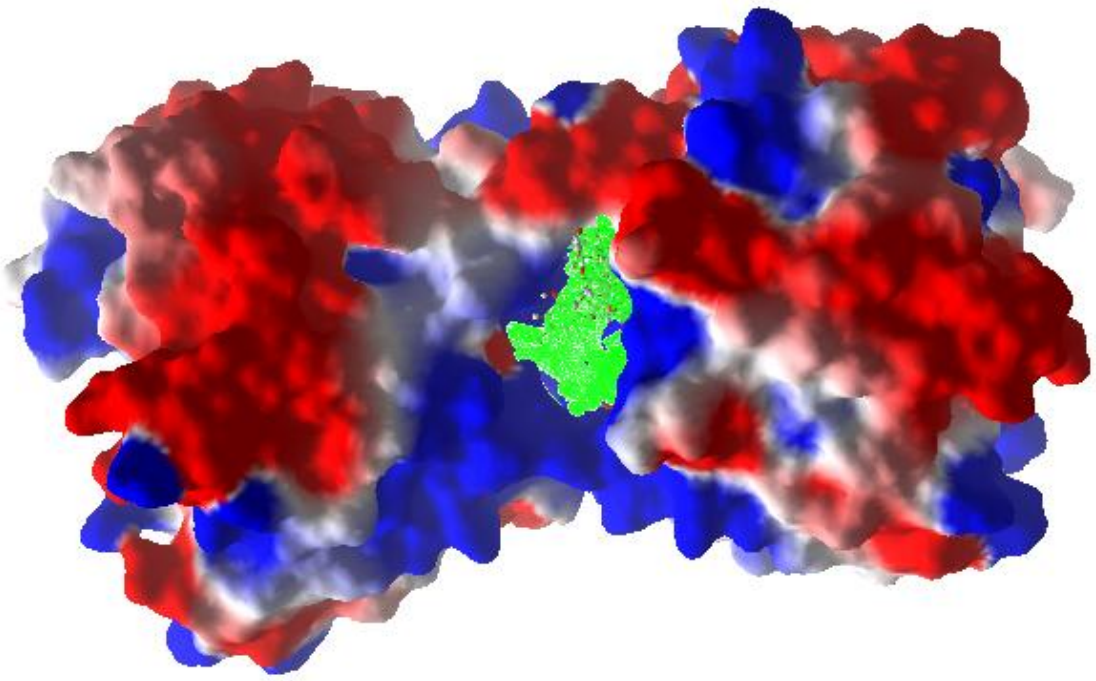

Figure 1. Electrostatic surface contours on the protein with the identified compounds in the optimum binding cavity

RESULTS AND DISCUSSION

After 14 days of treatment, the body weight in the control and three treatment groups did not differ significantly. Additionally, food and water intake remained similar across the groups. Therefore, the LD_{50} of the fraction is above 5000 mg/kg body weight. Hence, the extract is safe for consumption (Table 1). The markers of restoration of liver function following pretreatment with the *T. viride* flavonoid-rich fraction resulted in a strong dose-dependent hepatoprotective response to CCl_4-induced liver damage. In the positive control group, CCl_4 intoxication resulted in drastic increases in the levels of serum hepatic enzymes (ALT, AST, and ALP), which indicated extensive hepatocellular damage. Treatments with 200 mg/kg and 400 mg/kg flavonoid fractions significantly ($p<0.001$) reduced these elevated enzyme levels in a dose-dependent manner. However, the enzyme levels were not within the normal range, unlike the healthy negative control group (Table 1). These findings highlight the significant maintenance of liver cell membrane structure and activity. Table 2 shows that CCl_4 intoxication (positive control) caused a substantial decrease in the levels of the antioxidant enzymes catalase (CAT) and superoxide dismutase (SOD) and a significant increase in malondialdehyde (MDA), a major indicator of lipid peroxidation. The flavonoid-rich fractions of the *T. viride*-pretreated groups showed significant ($p<0.001$) decreases in the levels of serum hepatic enzymes at all doses. The significant increase in serum ALT, AST, ALP, CAT, and SOD levels induced by CCl_4 intoxication was ameliorated by pretreatment with the fractions in a dose-dependent manner, and this was accompanied by a significant reduction in MDA levels compared to the positive control group (Table 2).

The results indicate that CCl_4 intoxication in the positive control group caused extreme tissue damage, which is characterized by extreme necrosis (++ +), extremely ballooned cells (++ +), extreme central vein congestion (++ +), and a slight tendency toward inflammatory cells (+ +) (Table 3). Pretreatment with *T. viride* flavonoid fraction significantly reduced this damage in a dose-dependent manner. The treatment at 200 mg/kg BW changed severe parameters to mild levels (+), with necrosis, ballooning, and congestion, and the inflammatory cells were also mild (+). The increased dose of 400 mg/kg BW completely prevented congestion (0), further reduced necrosis to mild (+), but did not reduce ballooning, which remained moderate (++) (Table 3).

Histological examination of liver tissue revealed various morphological alterations in the experimental groups. The negative control group showed normal hepatic architecture with polygonal hepatocytes, intact cytoplasm, intact nuclei and nucleoli, and well-defined sinuoidal spaces, with no necrosis, ballooning, or inflammatory infiltration (Figure 2.A). Conversely, the positive control group presented severe histological damage, confirming that CCl_4 induced hepatotoxicity. It was characterized by massive necrosis, severe ballooning degeneration (fatty change), central vein congestion, architectural disorganization, and severe sinusoidal dilation (Figure 2.B). Pretreatment with the flavonoid-rich fraction significantly prevented this damage, and the liver sections showed a relatively intact parenchymal structure and hepatocyte integrity with only minor focal necrosis and minimal vacuolation in the diseased model (Figures 2.C and D).

Table 1. Clinical signs of toxicity of Wistar rats treated with *T. viride* flavonoid fraction

Group	Dose (mg/kg b.w.)	Feeding	Body weight (g)	Clinical signs of toxicity	No of animals dead
1	Vehicle	Normal	167±3.2	Normal	0/6
2	2000	Normal	165±4.1	Normal	0/6
3	5000	Normal	167±2.3	Normal	0/6

Note: Mg/kg b.w: Milligrams per kilogram of body weight

Table 2. Effects of the treatment of *T. viride* flavonoid fraction on oxidative stress markers in CCl_4-induced hepatotoxicity in rats

	200 mg/kg flavonoid-rich fraction	400 mg/kg flavonoid-rich fraction	Negative control	Positive control
ALT (U/L)	83.8±1.9$^{*\#}$	77.0±0.9$^{*\#}$	61.2±2.7	107.6±1.0$^{\#}$
AST (U/L)	35.6±1.6$^{*\#}$	29.60±0.4$^{*\#}$	19.2±1.2	42.0±1$^{\#}$
ALP (U/L)	238.6±6.1$^{*\#}$	218.2±4.2$^{*\#}$	99.6±0.9	318.4±1.7$^{\#}$
MDA (nmol/mL)	42.24±0.2$^{*\#}$	40.94±0.3$^{*\#}$	32.4±0.8	47.76±0.2$^{\#}$
CAT (U/mg protein)	28.24±0.4*	29.92±1*	38.98±0.9	15.58±0.9$^{\#}$
SOD (U/mg protein)	14.36±0.3$^{*\#}$	16.04±0.8$^{*\#}$	22.74±0.3	13.08±0.3$^{\#}$

Note: All values represent the mean ± SEM of n = 6. $p<0.001$, ANOVA, followed by Dunnett's multiple comparison test, compared with the positive (*) and negative (#) groups

Table 3. Histopathological scoring of liver tissue damage following CCl_4 intoxication

Groups	Tissue necrosis	Ballooned cells	Conjested Central veins	Inflammatory cells
Negative control	0	0	0	0
Positive control	+++	+++	+++	+
200 mg/kg flavonoid-rich fraction	+	+	+	+
400 mg/kg flavonoid-rich fraction	+	++	0	+

Note: 0: No changes, +: Mild, ++: Moderate, and +++: Severe changes

HPLC/MS profiles of the flavonoid-rich fraction of *T. viride*

HPLC-MS was used to identify ten flavonoids and riboflavin in the ethyl acetate fraction of *T. viride* (Figure 3), and the resulting spectra were compared with those of the literature and the LC-MS library. Compounds 1 (taxifolin, m/z 305.9) and 2 (daidzein, m/z 253) were also identified by water and proton ion losses as well as aglycone fragmentation. Glycosylated flavonoids, such as quercetin-3-O-neohesperidoside (compound 3, m/z 610.8), neodiosmin (compound 4, m/z 608.1), and isoamericanin-3-galactosyl-7-rhamnoside (compound 5, m/z 625.6), were detected with respect to neutral losses of rhamnosyl, neohesperidosyl, and galactosyl. Some other compounds include methoxyquercetin glycoside (compound 6, m/z 694.1), procyanidin B (compound 7, m/z 576.8), kaempferide (compound 8, m/z 300.1), kaempferol-3-O-xyloside (compound 9, m/z 418.8), riboflavin (compound 10, m/z 375.9), and nehesperidin (Table 4).

PASS online predicted hepatoprotective potential

Table 5 presents PASS online prediction results for the identified compounds as hepatoprotectants, expressed via probabilities of activity and inactivity. The values of Pa and Pi usually vary from 0.000 to 1.000, where Pa > Pi and Pa > 0.700. The compounds are considered physiologically promising in PASS analysis when Pa values exceed Pi values, especially when Pa > 0.7, suggesting a high likelihood of experimental activity. Most of the identified compounds had high Pa values with very low Pi values, as shown in Table 5, strongly indicating their hepatoprotective potential. The compounds with the highest probability of hepatoprotective activity were quercetin-3-O-neohesperidoside (Pa = 0.975, Pi = 0.001), neohesperidin (Pa = 0.982, Pi = 0.001), diosmetin-7-O-neohesperidoside (Pa = 0.967, Pi = 0.001), isohamnetin-3-galactoside-7-rhamnoside (Pa = 0.969, Pi = 0.001), and quercetin-3,7-dimethyl ether-3′-rutinoside (Pa = 0.973, Pi = 0.001). These high Pa values demonstrate strong confidence in their biological significance. Additionally, procyanidin B-type (Pa = 0.764) and taxifolin (Pa = 0.804) demonstrated significant predicted activities, suggesting their potential as cytoprotective and antioxidant agents. Kaempferol-3-O-xyloside (Pa = 0.902) provided additional support for the notion that flavonoid glycosides with possible hepatoprotective effects are common. Daidzein (Pa = 0.614) and kaempferide (Pa = 0.678), on the other hand, had moderate probabilities, indicating fewer but still conceivable hepatoprotective effects. The lack of predicted activity in PASS for riboflavin suggests that its hepatoprotective function may not be directly mediated by mechanisms the PASS algorithm identified.

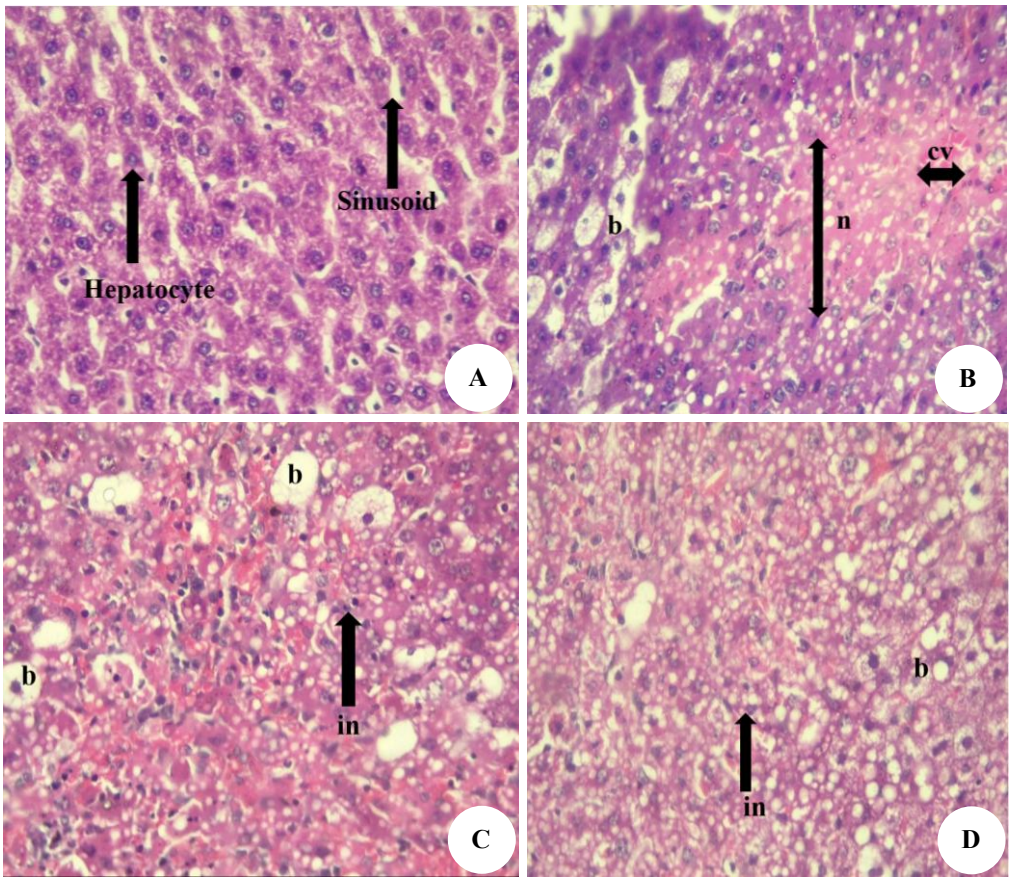

Figure 2. Light micrographs of the rat liver. A. Negative control, normal hepatocytes and sinusoids. B. Positive control, parenchymal architecture disruption, and dilatation of sinusoids. C. 200 mg/kg flavonoid-rich fraction. D. 400 mg/kg flavonoid-rich fraction, few ballooned cells and inflammatory cells (H&E ×400). Note: n: Necrotic, b: Ballooned cells, cv: Central vein, in: Ballooned and necrotic hepatocytes with numerous inflammatory cells

Table 4. High-performance liquid chromatography/mass spectrometry identification of the flavonoid fractions of *T. viride*

S/No	RT (min)	Fragmentation pattern (m/z)	Compounds detected	Chemical Structure	Compound Class
1	1.538	305.9, 304.7, 287.9, 259.9	Taxifolin (Dihydroquercetin)	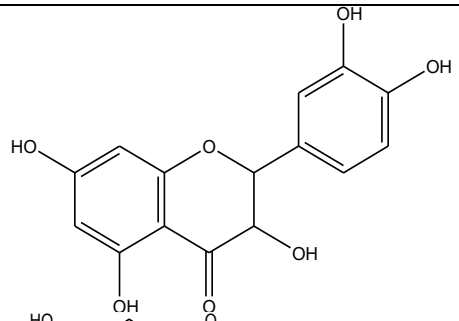	Flavonoids (flavonol)
2	3.835	253.0, 251.5, 235.3	Daidzein (7,4′-dihydroxyisoflavone)	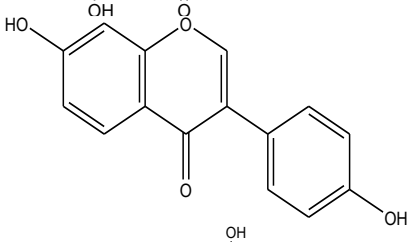	Flavonoids (Isoflavone)
3	9.498	610.8, 464.7, 302.8	Quercetin-3-O-neohesperidoside	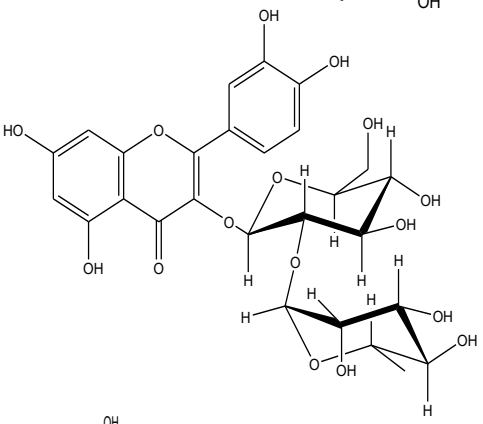	Flavonoids (Flavonol) glycoside
4	11.348	608.1, 594.1, 283.1, 146.0	Diosmetin-7-O-neohesperidoside (Neodiosmin)	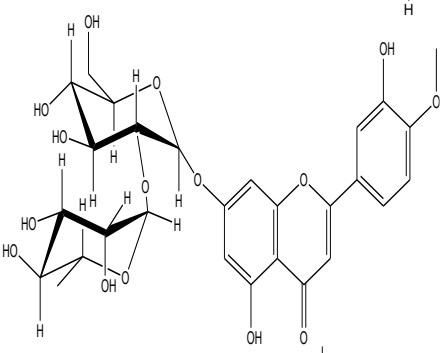	Flavonoids (flavone) glycoside
5	12.487	625.6, 478.6, 316.9, 147.7	Isohamnetin-3-galactoside-7-rhamnoside	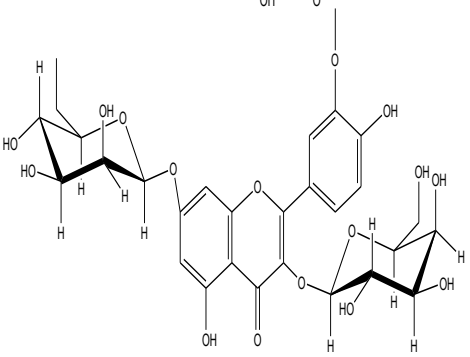	Flavonoids (flavonol) glycoside

6	14.108	694.1, 382.7, 301.7, 284.1	Quercetin-3,7-dimethyl ether-3'-rutinoside	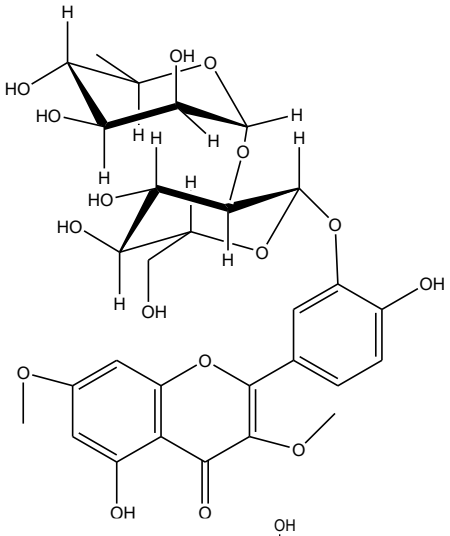	Flavonoids (flavonol) glycoside
7	16.227	576.8, 426.0, 289.9	Procyanidin (B-type)	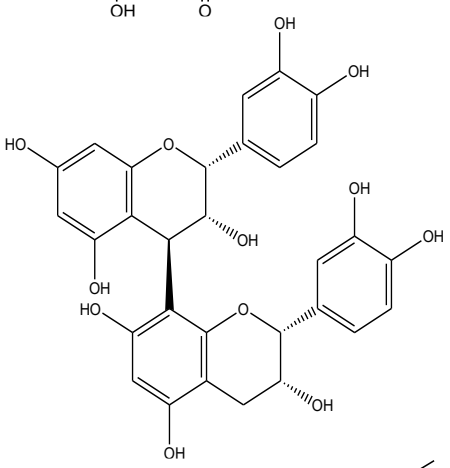	Flavonoids (Biflavonoid)
8	17.480	300.8, 300.1, 299.0, 285.7	Kaempferide	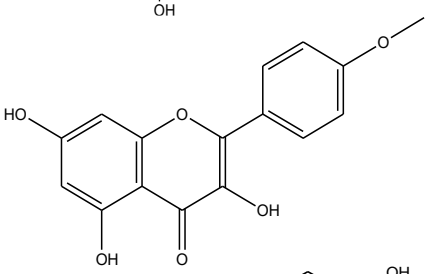	Flavonoids (flavonol)
9	18.539	441.0, 418.8, 287.6	Kaempferol-3-O-xyloside	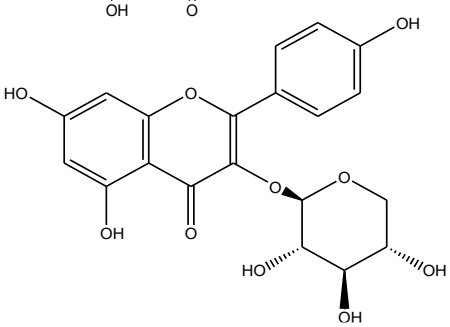	Flavonoids (flavonol) glycoside

10	19.121	375.9, 242.0, 117.9	Riboflavin	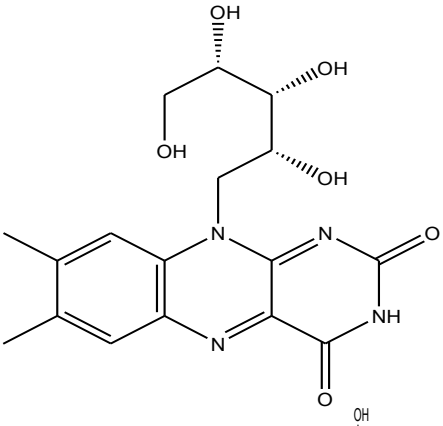	Vitamin
11	20.441	611.0, 465.0, 402.9, 302.0, 151.9	Neohesperidin	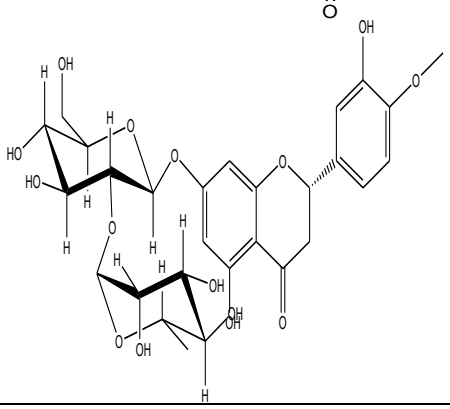	Flavonoids (flavanone) glycoside

Table 5. Predicted pharmacological potential of the identified compounds as hepatoprotectants

Identified compound	Compounds detected	Probability "to be active" (Pa)	Probability "to be inactive"(Pi)
1	Taxifolin (Dihydroquercetin)	0.804	0.004
2	Daidzein (7-hydroxy-3-(4-hydroxyphenyl)-4H-chromen-4-one)	0.614	0.011
3	Quercetin-3-O-neohesperidoside	0.975	0.001
4	Diosmetin-7-O-neohesperidoside (Neodiosmin)	0.967	0.001
5	Isohamnetin-3-galactoside-7-rhamnoside	0.969	0.001
6	Quercetin-3,7-dimethyl ether-3'-rutinoside	0.973	0.001
7	Procyanidin (B-type)	0.764	0.005
8	Kaempferide	0.678	0.008
9	Kaempferol-3-O-xyloside	0.902	0.002
10	Riboflavin	-	-
11	Neohesperidin	0.982	0.001

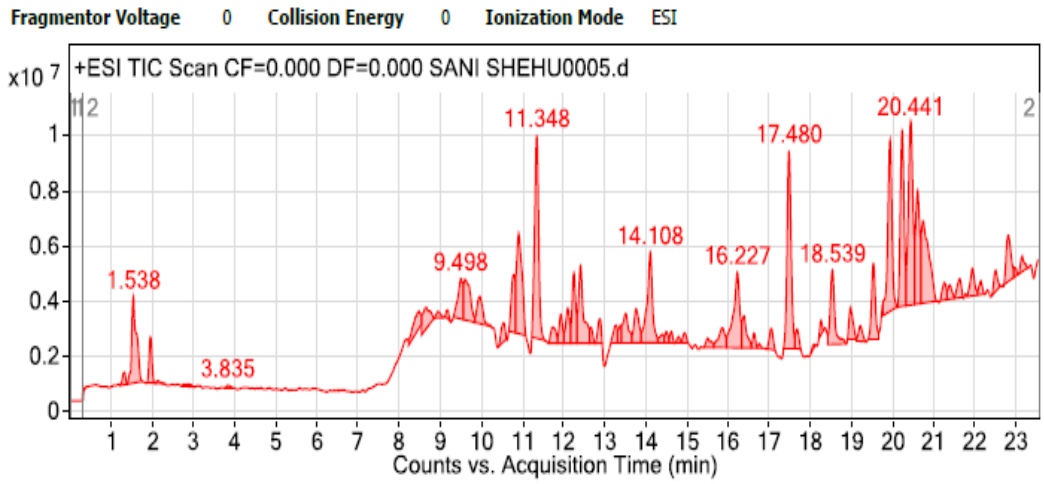

Figure 3. Chromatogram profile of the flavonoid-rich fraction of *T. viride*

Molecular docking results

Molecular docking experiments were performed against the Keap1 target protein (PDB: 4L7B) to elucidate the molecular basis of the expected hepatoprotective effect. Table 6 summarizes the docking results, including the MolDock score, rerank score, and hydrogen-bonding energy. All the identified compounds had high binding affinities for the Keap1 protein, with MolDock scores ranging from -100.61 to -177.57 kcal/mol, indicating stable ligand–protein complexes. Isohamnetin-3-galactoside-7-rhamnoside had the greatest interaction with Keap1, with the highest binding activity (MolDock score = -177.57 kcal/mol) and the best hydrogen bond contribution (-26.11 kcal/mol). The amino acid residues involved in the molecular interactions of the ishamnetin-3-galactoside-7-rhamnoside complex include ARG B: 483, ARG B: 415, SER B: 508, GLY B: 462, GLY B: 367, GLY B: 509, GLY B: 603, ALA B: 556, ALA B: 510, ILE B: 559, VAL B: 606, and VAL B: 604. Additionally, the procyanidin (B-type) complex with a MolDock score = -162.24 kcal/mol had residual interactions with PRO A: 384, ARG A: 380, TYR B: 334, SER B: 602, ARG B: 380, ARG B: 415, ASN B: 414, and ASN B: 387. This finding indicates a highly stable binding state characterized by strong hydrogen-bonding interactions within the Keap1 binding pocket. Similarly, quercetin-3,7-dimethyl ether-3′-rutinoside, procyanidin B-type, and quercetin-3-O-neohesperidoside presented strong MolDock scores of -161.69, -162.24, and -156.63 kcal/mol, respectively, accompanied by significant hydrogen bond energies. These values were much higher than those of the reference compounds (MolDock score = -136.01 kcal/mol), indicating better binding affinity and stability. Notably, diosmetin-7-O-neohesperidoside (-135.98 kcal/mol) and neohesperidin (-135.73 kcal/mol) have MolDock scores equivalent to those of the reference ligand, indicating their ability to bind to the Keap1 active site. Even molecules with modest PASS scores, such as taxifolin, daidzein, and kaempferide, showed favorable docking energies and hydrogen-bonding interactions, suggesting they may still contribute to the overall biological impact through molecular contact with Keap1. The rerank scores presented in Table 6 indicate the stability of the docked complexes, with significantly negative values indicating favorable binding postures following energy refinement. The high hydrogen bonding energies reported across numerous compounds highlight the role of polar interactions in stabilizing ligand binding within the Keap1 Kelch domain (Figure 4).

Table 6. Binding affinity scores of the identified compounds with the crystal structure of the Keap1 target (PDB: 4L7B)

Identified compound	Compounds names	MolDock Score (kcal/mol)	Rerank Score	HBond (kcal/mol)
1	Taxifolin (Dihydroquercetin)	-100.61	-90.76	-7.58
2	Daidzein (7-hydroxy-3-(4-hydroxyphenyl)-4H-chromen-4-one)	-101.39	-31.75	-7.30
3	Quercetin-3-O-neohesperidoside	-156.63	-122.68	-17.69
4	Diosmetin-7-O-neohesperidoside (Neodiosmin)	-135.98	-126.90	-6.39
5	Isohamnetin-3-galactoside-7-rhamnoside	**-177.57**	**-162.92**	**-26.11**
6	Quercetin-3,7-dimethyl ether-3’-rutinoside	-161.69	-124.07	-22.26
7	Procyanidin (B-type)	**-162.24**	**-116.99**	**-18.54**
8	Kaempferide	-106.73	-90.68	-11.40
9	Kaempferol-3-O-xyloside	-115.33	-106.79	-10.61
10	Riboflavin	-101.85	-66.60	-7.21
11	Neohesperidin	-135.73	-111.31	-3.73
Reference compound	(1S,2R)-2-(Mathes et al. 2025-dihydroisoquinolin-2(1H)-yl]carbonyl)cyclohexanecarboxylic acid	-136.01	-109.76	-1.70

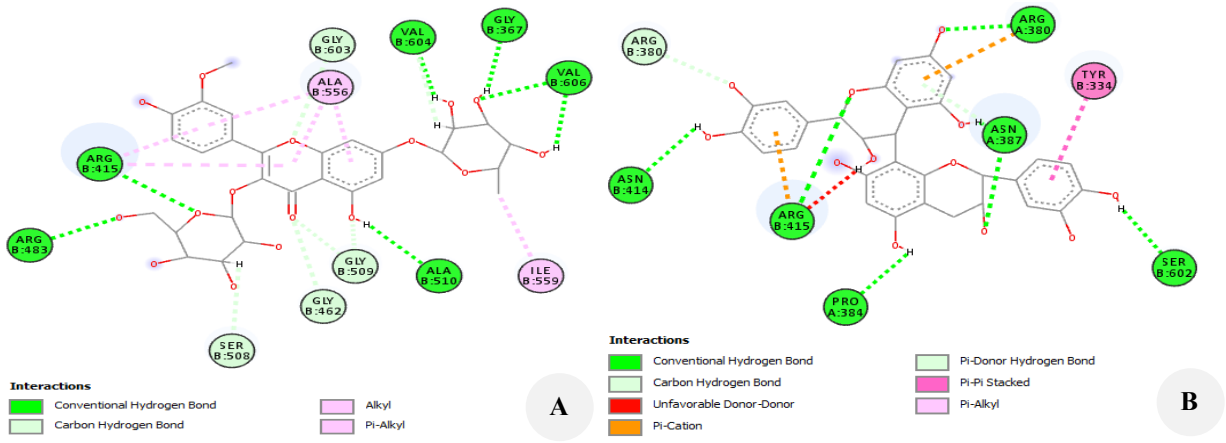

Figure 4. 2D residual interactions of the identified compounds with the Keap1 domain, PDB: 4L7B. A. Compound 5: ishamnetin-3-galactoside-7-rhamnoside complex, B. Compound 7: procyanidin (B-type)

In vivo and in silico hepatoprotective correlations of the *T. viride* flavonoid fraction

The in vivo hepatoprotective activity of the *T. viride* flavonoid fraction is strongly supported by in silico data. The normalization of serum biomarker fractions (ALT, AST, and ALP), oxidative stress markers (MDA, CAT, and SOD), and liver histopathology in CCl4-treated rats is consistent with the highly predictive pharmacological potential and favorable molecular docking properties. The in vivo hepatoprotective action is correlated with high probability of activity (Pa) values for most of the identified compounds, as determined using PASS online prediction. The highest Pa values are the primary contributors to the fraction's potent effect. The in silico prediction indicated a significant decrease in hepatic necrosis and enzyme leakage in the treatment groups, suggesting that the compounds activate hepatoprotective pathways. Compounds with intermediate Pa values exhibit a synergistic effect. The high binding affinities (MolDock scores from -100.61 to -177.57 kcal/mol) of the flavonoid compounds to the Keap1 protein (PDB: 4L7B) suggest direct interference with the Keap1-Nrf2 interaction. Interfering with this complex is an established way to stimulate the Nrf2 pathway, thereby protecting endogenous antioxidant enzymes such as CAT and SOD. These findings are highly consistent with the in vivo results, which showed that pretreatment with the flavonoid fraction significantly increased CAT and SOD levels and decreased lipid peroxidation (MDA) in CCl_4-treated rats. Therefore, a clear and rational correlation exists: the in silico results successfully confirmed that the *T. viride* fraction has a high probability of hepatoprotective activity.

Discussion

The fraction shows a positive safety profile as there are no significant differences in body weight, food intake, or water consumption between groups during the 14-day study period (Schlede 2002; Akhila et al. 2007). The estimated median Lethal Dose (LD_{50}) is greater than 5000 mg/kg body weight; the extract is considered safe because it may be consumed orally. The carbon tetrachloride (CCl_4)-induced hepatotoxicity model is an established and relevant model for assessing hepatoprotective agents because the mechanism of pathogenesis of the model involves bioactivation of the cytochrome P450-mediated production of the trichloromethyl radical (CCl_3), which is typical of oxidative stress and necroinflammatory cascades in human diseases such as viral hepatitis and Drug-Induced Liver Injury (DILI) (Mrwad et al. 2025). These radicals trigger a self-sustaining wave of lipid peroxidation that directly impairs the phospholipid bilayer of hepatocellular and organelle membranes (Halliwell and Chirico 1993). This resulting increase in membrane permeability results in the characteristic efflux of intracellular enzymes, such as ALT and AST, into the circulation, which are essential biochemical indicators of cytotoxicity and loss of functional integrity (Túnez et al. 2005). This phenomenon is histologically characterized by centrilobular necrosis, ballooning of hepatocytes (steatosis), sinusoidal dilation, and inflammation, which have been conclusively demonstrated in our positive control group and widely supported in the literature (Muriel 2009; Dutta et al. 2018). Our results indicate that prior exposure to the flavonoid-rich fraction of *T. viride* provides substantial dose-dependent protection against this multifaceted damage. The significant reduction in serum enzyme elevation and simultaneous increase in histopathological scores, i.e., a decrease in severe (+++) to mild (+) necrosis and avoidance of central vein congestion with a 400 mg/kg dose, are strong in vivo evidence of its effectiveness. It indicates that the fraction not only serves as a palliative but also engages the core pathogenic pathway, most likely by stabilizing the membrane architecture and/or escalating endogenous regenerative mechanisms (Fujiyoshi and Ozaki 2011). Taxifolin (dihydroquercetin), daidzein, and quercetin-3-O-neohesperidoside exhibit significant hepatoprotective effects through their antioxidant and anti-inflammatory properties, as evidenced by decreased markers of oxidative stress and by inhibition of NF-κB-stimulated cytokine synthesis in preclinical models (Alanezi et al. 2022; Dogara et al. 2025). In addition, flavonoids such as kaempferide, quercetin-3,7-dimethyl ether-3'-rutinoside, and riboflavin play a role in cytoprotection by increasing endogenous antioxidant responses, specifically via the Nrf2 pathway and the modulation of the gut-liver axis, and neohesperidin specifically suppresses drug-induced hepatotoxicity through the inhibition of inflammatory and angiogenic pathways (Solanki et al. 2024). The identification of common flavonoid aglycone bases and their glycosidic conjugates is consistent with the established phytochemistry of the Thesium genus, which is abundant in phenolic acids and flavonols (Lombard et al. 2022). Although kaempferide and quercetin were previously identified in *T. viride* (Shehu et al. 2016), taxifolin, daidzein, procyanidin and kaempferol have been reported in this plant. This increased profile is of essential importance, since the concerted effort of these compounds may be used to account for the observed hepatoprotection by well-established pathways: free radical scavenging, CYP2E1 enzyme charge that activates CCl_4, inhibition of the NF-kB-based inflammatory pathway, and upregulation of antioxidant enzymes such as SOD and CAT (Nijveldt et al. 2001; Gajender et al. 2023).

The majority of the compounds have consistently low Pi values, which indicates a very low probability of inactivity. The PASS results indicate that flavonoids and polyphenolic glycosides, well recognized for their antioxidant, free radical-scavenging, and cytoprotective properties, are the main drivers of the extract's hepatoprotective effects. In docking simulations, the identified compounds with favorable PASS-predicted hepatoprotective probabilities were in agreement with their binding affinities to the Keap1 domain. Thus, the compounds bind to the domain to determine whether they might directly block the protein-protein interaction between Keap1 and Nrf2. Numerous known inhibitors that directly bind to the Kelch domain of Keap1, which is thought to be the Nrf2 peptide binding site, disrupt the Nrf2-Keap1 relationship and promote Nrf2 nuclear translocation (Yang

et al. 2025). The Nrf2 activation caused by our identified compounds could be linked to direct binding to the Kelch domain of Keap1 (Jnoff et al. 2014). Keap1 is essential for the proper function of the Nrf2 antioxidant pathway. Strong binding of flavonoid glycosides, for example, to Keap1 may disrupt the Keap1-Nrf2 interaction, increasing Nrf2 activation and the overexpression of antioxidant and cytoprotective enzymes such as heme oxygenase (Zhou et al. 2019). The in vivo hepatoprotective properties of the *T. viride* flavonoid fraction are directly related to molecular docking predictions in which the identified compounds showed high binding affinity.

The flavonoid-rich fraction reduced excessive hepatic necrosis, vacuolation, ballooning, central vein congestion, and inflammatory cell infiltration associated with CCl_4-induced liver injury. The *S. viride* flavonoid fraction exhibited strong hepatoprotective effects, which were corroborated by computational docking.

In conclusion, the current research confirms the conventional application of *T. viride* in the treatment of liver diseases. The fraction was found to decrease serum liver enzymes, strongly inhibit oxidative stress markers, restore endogenous antioxidant defenses, and direct pathological confirmation of reduced hepatocellular necrosis, vacuolation, and architectural injury. Chemical composition analysis revealed the presence of eleven bioactive compounds. In silico assessments of the PASS online results revealed that the identified compounds had high predicted hepatoprotective potential. Additionally, the consistently high MolDock scores, favorable rerank values, and robust hydrogen-bonding interactions show that the identified flavonoids, particularly isorhamnetin-3-galactoside-7-rhamnoside and procyanidin B-type, can effectively bind Keap1, suggesting their mechanistic role in hepatoprotection.

Future studies should use a large sample size and a standard drug to compare fraction efficacy. A control group with a high dose of the fraction should also be included in the experimental design. Flavonoid identification in this study was performed by comparing chromatographic and spectral data with databases. In future research, emphasis should be placed on isolating individual compounds and determining them definitively using valid analytical methods. This approach will identify specific bioactive compounds, enabling standard formulations and comprehensive mechanistic investigations. Direct molecular validation of Keap1-Nrf2 should be evaluated. Additionally, subacute toxicity studies of the *T. viride* flavonoid fraction should be conducted to assess its safety and effects on the other organs.

REFERENCES

Abdou EM, Fayed MA, Helal D, Ahmed KA. 2019. Assessment of the hepatoprotective effect of developed Lipid-Polymer Hybrid Nanoparticles (LPHNPs) encapsulating naturally extracted β-sitosterol against CCl4-induced hepatotoxicity in rats. Sci Rep 9 (1): 19779. https://doi.org/10.1038/s41598-019-56320-2.

Abdullahi M, Uzairu A, Shallangwa GA, Mamza PA, Ibrahim MT, Chandra A, Goel VK. 2024. In-silico molecular modeling studies of some camphor imine based compounds as anti-influenza A (H1N1) pdm09 virus agents. J Biomol Struct Dyn 42 (4): 2013-2033. https://doi.org/10.1080/07391102.2023.2209654.

Abdullahi M, Uzairu A, Shallangwa GA, Mamza PA, Ibrahim MT, Chandra A, Goel VK. 2025. Molecular modeling studies of substituted indole derivatives as novel influenza A virus inhibitors. J Biomol Struct Dyn 43 (1): 241-260. https://doi.org/10.1080/07391102.2023.2280735.

Abdulrahman MD, Bradosty SW, Hamad SW, Ibrahim MT, Lema AA, Sunusi N, Usman M, Ashiru I, Ahmad NB, Wada N, Bussman RW. 2022. Traditional methods for treatment and management of measles in Northern Nigeria: Medicinal plants and their molecular docking. Ethnobot Res Appl 23: 1-18. https://dx.doi.org/10.32859/era.23.33.1-18.

Agati G, Brunetti C, Fini A, Gori A, Guidi L, Landi M, Sebastiani F, Tattini M. 2020. Are flavonoids effective antioxidants in plants? Twenty years of our investigation. Antioxidants 9 (11): 1098. https://doi.org/10.3390/antiox9111098.

Akhila JS, Shyamjith D, Alwar M. 2007. Acute toxicity studies and determination of median lethal dose. Curr Sci 93 (7): 917-920.

Alanezi AA, Almuqati AF, Alfwuaires MA, Alasmari F, Namazi NI, Althunibat OY, Mahmoud AM. 2022. Taxifolin prevents cisplatin nephrotoxicity by modulating Nrf2/HO-1 pathway and mitigating oxidative stress and inflammation in mice. Pharmaceuticals 15 (11): 1310. https://doi.org/10.3390/ph15111310.

Chattopadhyay RR. 2003. Possible mechanism of hepatoprotective activity of *Azadirachta indica* leaf extract: Part II. J Ethnopharmacol 89 (2-3): 217-219. https://doi.org/10.1016/j.jep.2003.08.006.

Chowdhury AB, Mehta KJ. 2023. Liver biopsy for assessment of chronic liver diseases: A synopsis. Clin Exp Med 23 (2): 273-285. https://doi.org/10.1007/s10238-022-00799-z.

Dogara AM, Bradosty SW, Al-Zahrani AA, Hamad SW, Almalki HD. 2025. Ethnobotany, bioactive compounds and pharmacology of *Syzygium guineense* (Willd.) DC: A review. J Ethnopharmacol 339: 119149. https://doi.org/10.1016/j.jep.2024.119149.

Dogara AM, Ibrahim MT, Mahmud AA, Danladi MD, Lema AA, Muhammad U, Tahir AS. 2024. Antioxidant, alpha glucosidase inhibition, chemical composition, and molecular docking of *Thesium viride* AW Hill. Arab J Med Aromat Plant 10 (1): 1-19. https://doi.org/10.48347/IMIST.PRSM/ajmap-v10i1.45992.

Dutta S, Chakraborty AK, Dey P, Kar P, Guha P, Sen S, Kumar A, Sen A, Chaudhuri TK. 2018. Amelioration of CCl_4-induced liver injury in Swiss albino mice by antioxidant-rich leaf extract of *Croton bonplandianus* Baill. PLoS ONE 13 (4): e0196411. https://doi.org/10.1371/journal.pone.0196411.

Etame RME, Mouokeu RS, Poundeu FSM, Voukeng IK, Cidjeu CLP, Tiabou AT, Yaya AJG, Ngane RAN, Kuiate JR, Etoa FX. 2019. Effect of fractioning on antibacterial activity of n-butanol fraction from *Enantia chlorantha* stem bark methanol extract. BMC Complement Alternat Med 19 (1): 56. https://doi.org/10.1186/s12906-019-2459-y.

Fujiyoshi M, Ozaki M. 2011. Molecular mechanisms of liver regeneration and protection for treatment of liver dysfunction and diseases. J Hepato-Biliary-Pancreat Sci 18 (1): 13-22. https://doi.org/10.1007/s00534-010-0304-2.

Gajender, Mazumder A, Sharma A, Azad MA. 2023. A comprehensive review of the pharmacological importance of dietary flavonoids as hepatoprotective agents. Evid Base Complement Alternat Med 2023: 4139117. https://doi.org/10.1155/2023/4139117.

Halliwell B, Chirico S. 1993. Lipid peroxidation: Its mechanism, measurement, and significance. Am J Clin Nutr 57 (5): 715S-725S. https://doi.org/10.1093/ajcn/57.5.715S.

Huang DQ, Wong VW, Rinella ME, Boursier J, Lazarus JV, Yki-Järvinen H, Loomba R. 2025. Metabolic dysfunction-associated steatotic liver disease in adults. Nat Rev Dis Primer 11 (1): 14. https://doi.org/10.1038/s41572-025-00599-1.

Jnoff E, Albrecht C, Barker JJ, Barker O, Beaumont E, Bromidge S, Brookfield F, Brooks M, Bubert C, Ceska T, Corden V, Dawson G, Duclos S, Fryatt T, Genicot C, Jigorel E, Kwong J, Maghames R, Mushi I, Pike R, Sands ZA, Smith MA, Stimson CC, Courade J-P. 2014. Binding mode and structure-activity relationships around direct inhibitors of the Nrf2-Keap1 complex. Chem Med Chem 9 (4): 699-705. https://doi.org/10.1002/cmdc.201300525.

Kaur A, Kumar A, Walia H, Khosla S. 2025. Comprehensive study on phytochemical constituents and bioactive potential of aerial part extracts of *Strobilanthes attenuata*: An underexplored medicinal

plant. R Square Preprint (2025): 1-50. https://doi.org/10.21203/rs.3.rs-8289255/v1.

Liu Y-B, Chen M-K. 2022. Epidemiology of liver cirrhosis and associated complications: Current knowledge and future directions. World J Gastroenterol 28 (41): 5910-5930. https://doi.org/10.3748/wjg.v28.i41.5910.

Lombard N, Stander MA, Redelinghuys H, Le Roux MM, van Wyk B-E. 2022. A study of phenolic compounds and their chemophenetic value in the genus *Thesium* (Santalaceae). Diversity 14 (8): 590. https://doi.org/10.3390/d14080590.

Lombard N, van Wyk B-E, le Roux MM. 2020. A review of the ethnobotany, contemporary uses, chemistry and pharmacology of the genus *Thesium* (Santalaceae). J Ethnopharmacol 256: 112745. https://doi.org/10.1016/j.jep.2020.112745.

Mathes D, Macedo LB, Pieta TB, Machado MM, Rodrigues OED, Leal JG, da Silva SR, Librelotto GR, Rolim CMB, Librelotto DRN. 2025. Exploring ADMET properties and the anticancer potential mechanism of a new organoselenium compound using network pharmacology and in vitro study. Ciênc Nat 47: e88474. https://doi.org/10.5902/2179460X88474.

Morris-Schaffer K, McCoy MJ. 2020. A review of the LD_{50} and its current role in hazard communication. ACS Chem Health Saf 28 (1): 25-33. https://doi.org/10.1021/acs.chas.0c00096.

Mrwad AA, El-Shafey S, Said NM. 2025. Carbon tetrachloride: A classic model for liver toxicity. Biochem Lett 21 (1): 1-10. https://doi.org/10.21608/blj.2025.381090.1070.

Muriel P. 2009. Role of free radicals in liver diseases. Hepatol Intl 3 (4): 526-536. https://doi.org/10.1007/s12072-009-9158-6.

Nagalekshmi R, Menon A, Chandrasekharan DK, Nair CKK. 2011. Hepatoprotective activity of *Andrographis paniculata* and *Swertia chirayita*. Food Chem Toxicol 49 (12): 3367-3373. https://doi.org/10.1016/j.fct.2011.09.026

Negi AS, Kumar J, Luqman S, Shanker K, Gupta M, Khanuja S. 2008. Recent advances in plant hepatoprotectives: A chemical and biological profile of some important leads. Med Res Rev 28 (5): 746-772. https://doi.org/10.1002/med.20115.

Nijveldt RJ, Van Nood E, Van Hoorn DE, Boelens PG, Van Norren K, Van Leeuwen PA. 2001. Flavonoids: A review of probable mechanisms of action and potential applications. Am J Clin Nutr 74 (4): 418-425. https://doi.org/10.1093/ajcn/74.4.418.

Paik JM, Golabi P, Younossi Y, Mishra A, Younossi ZM. 2020. Changes in the global burden of chronic liver diseases from 2012 to 2017: The growing impact of NAFLD. Hepatology 72 (5): 1605-1616. https://doi.org/10.1002/hep.31173.

Prata JC, Da Costa JP, Lopes I, Duarte AC, Rocha-Santos T. 2020. Environmental exposure to microplastics: An overview on possible human health effects. Sci Total Environ 702: 134455. https://doi.org/10.1016/j.scitotenv.2019.134455.

Schlede E. 2002. Oral acute toxic class method: OECD Test Guideline 423. Rapporti Istisan 41: 32-36.

Shehu S, Abubakar M, Ibrahim G, Iliyasu U. 2016. Phytochemical and antibacterial studies on aqueous ethanol extract of *Thesium viride* (Santalaceae). Br J Pharm Res 11 (4): 1-7. https://doi.org/10.9734/BJPR/2016/23046.

Shehu S, Ibrahim G, Iliyasu U, Nuhu A, Abubakar M. 2017. Evaluation of antiulcer activity of aqueous ethanol extract of *Thesium viride* on ethanol and aspirin induced models in rats. Bayero J Pure Appl Sci 9 (2): 82-85. http://dx.doi.org/10.4314/bajopas.v9i2.16.

Shehu S, Iliyasu U, Waziri P, Abdulrazak A, Ajibesin KK. 2025. Chromatographic and spectroscopic characterization and identification of compounds in flavonoid-rich fraction of *Thesium viride* AW Hill. UMYU Sci 4 (2): 298-308. https://doi.org/10.56919/usci.2542.029.

Shi X, Zhu X, Jiang Q, Ma T, Du Y, Wu T. 2023. Determination of contaminants in polyolefin recyclates by High-Performance Liquid Chromatography-Mass Spectrometry (HPLC-MS). Anal Lett 56 (5): 758-768. https://doi.org/10.1080/00032719.2022.2101656.

Solanki K, Patel J, Desai D, Chaudhari M. 2024. Protective effect quercetin on methotrexate induced toxicity in Wistar rats. Intl J Pharm Sci Res 15 (9): 2709-2718. https://doi.org/10.13040/IJPSR.0975-8232.15(9).2709-18.

Talli I, Marchioro L, Zaninotto M, Cosma C, Pangrazzi E, Artusi C, Padoan A, Plebani M. 2025. Measurement of AST and ALT with Pyridoxal-5′-Phosphate according to IFCC: A decades-long gap seems to be filled. Clin Chimic Acta 569: 120158. https://doi.org/10.1016/j.cca.2025.120158.

Tapper EB, Parikh ND. 2023. Diagnosis and management of cirrhosis and its complications: A review. JAMA 329 (18): 1589-1602. https://doi.org/10.1001/jama.2023.5997.

Túnez I, Muñoz MC, Villavicencio MA, Medina FJ, de Prado EP, Espejo I, Barcos M, Salcedo M, Feijóo M, Montilla P. 2005. Hepato-and neurotoxicity induced by thioacetamide: Protective effects of melatonin and dimethylsulfoxide. Pharmacol Res 52 (3): 223-228. https://doi.org/10.1016/j.phrs.2005.03.007.

Venmathi MBA, Iqbal M, Gangadaran P, Ahn B-C, Rao PV, Shah MD. 2022. Hepatoprotective potential of Malaysian medicinal plants: A review on phytochemicals, oxidative stress, and antioxidant mechanisms. Molecules 27 (5): 1533. https://doi.org/10.3390/molecules27051533.

Yang LL. 2020. Anatomy and physiology of the liver. In: Milan Z, Goonasekera C (eds.). Anesthesia for Hepatico-Pancreatic-Biliary Surgery and Transplantation. Springer, Cham. https://doi.org/10.1007/978-3-030-51331-3_2.

Yang X, Liu Y, Cao J, Wu C, Tang L, Bian W, Chen Y, Yu L, Wu Y, Li S. 2025. Targeting epigenetic and post-translational modifications of NRF2: Key regulatory factors in disease treatment. Cell Death Discov 11 (1): 189. https://doi.org/10.1038/s41420-025-02491-z.

Zhigila DA, Verboom GA, Muasya AM. 2020. An infrageneric classification of *Thesium* (Santalaceae) based on molecular phylogenetic data. Taxon 69 (1): 100-123. https://doi.org/10.1002/tax.12202.

Zhou Y, Jiang Z, Lu H, Xu Z, Tong R, Shi J, Jia G. 2019. Recent advances of natural polyphenols activators for Keap1-Nrf2 signaling pathway. Chem Biodiver 16 (11): e1900400. https://doi.org/10.1002/cbdv.201900400.